



HAL
open science

Rotational Doppler effect on reflection upon an ideal rotating propeller

Olivier Emile, J. Emile, Christian Brousseau, T. Le Guennic, P. Jian, G. Labroille

► **To cite this version:**

Olivier Emile, J. Emile, Christian Brousseau, T. Le Guennic, P. Jian, et al.. Rotational Doppler effect on reflection upon an ideal rotating propeller. *Journal of the Optical Society of America B*, 2022, 39 (7), pp.1945-1949. 10.1364/JOSAB.461445 . hal-03718141

HAL Id: hal-03718141

<https://hal.science/hal-03718141>

Submitted on 14 Oct 2022

HAL is a multi-disciplinary open access archive for the deposit and dissemination of scientific research documents, whether they are published or not. The documents may come from teaching and research institutions in France or abroad, or from public or private research centers.

L'archive ouverte pluridisciplinaire **HAL**, est destinée au dépôt et à la diffusion de documents scientifiques de niveau recherche, publiés ou non, émanant des établissements d'enseignement et de recherche français ou étrangers, des laboratoires publics ou privés.

Rotational Doppler effect on reflection upon an ideal rotating propeller

OLIVIER EMILE^{1,*}, JANINE EMILE², CHRISTIAN BROUSSEAU³, TANGI LE GUENNIC⁴, PU JIAN⁴, AND GUILLAUME LABROILLE⁴

¹ Université de Rennes 1, Campus de Beaulieu, F-35000 Rennes, France

² Université de Rennes 1, CNRS IPR UMR 6251, F-35000 Rennes, France

³ Université de Rennes 1, CNRS IETR UMR 6164, F-35000 Rennes, France

⁴ CAILabs, 38 boulevard Albert 1^{er}, F-35200 Rennes, France

* olivier.emile@univ-rennes1.fr

The rotational Doppler shift is the counterpart of the usual linear Doppler effect for rotating bodies. We study by an experimental approach coupled with theoretical considerations the rotational shift of a fundamental laser light reflected on an ideal rotating propeller. We decompose the reflected light on a Laguerre Gaussian basis and show that only the modes having the same rotational symmetry as the propeller are involved in the decomposition. The latter experience a frequency shift proportional to the rotation frequency of the propeller and the topological charge of the beam. Extensions of this work in the microwave domain are then considered.

1. INTRODUCTION

A monostatic Doppler radar is a system where both the emitter and the receiver are co-located. This is the conventional configuration for a radar [1, 2]. As various elements within a target experience oscillatory movement, frequency modulations around the carrier frequency of the main reflected sensor signals are induced. They are called micro-Doppler signals [3, 4]. A rotating target also induces micro-Doppler effects that are used to characterize its rotation [4]. However, it is difficult to isolate them from other micro-Doppler peaks due to pure vibrations, and thus to fully identify the rotation. On the other hand, it exists a so-called rotational Doppler shift. It arises from the rotational motion between the transmitter, also called the source and the receiver also called the observer [5]. It is the counterpart of the linear Doppler effect for rotating bodies. Many possible applications have already been considered to track rotational motion [6]. Nevertheless, during interaction with the rotating body, the total angular momentum of the electromagnetic field has to change [7]. Therefore, in reflection, the rotational Doppler effect has been limited to the scattering by rough surfaces [8–10], or to the reflection on phase conjugated mirrors [11], metasurfaces and helicoidal reflectors [12, 13] or prisms [14]. Very recently, it has been shown that a rotational Doppler shift can be isolated in the decomposition of the image of an object having a rotational symmetry in a bistatic configuration [15–17]. Then, the ques-

tion arises whether the decomposition of the usual fundamental beam reflected on a rotating object could induce rotational Doppler shifts that could be measured, enabling unambiguously rotation identification. The aim of this article is thus to investigate the frequency shifts of the light reflected by a rotating object having rotational symmetry.

2. EXPERIMENTAL SET-UP

The experimental set-up is depicted in Fig. 1. The light from an eye-safe infrared laser (CEFL Keopsys, $\lambda=1.55 \mu\text{m}$, connected to a single mode fiber SMF-28) is sent to the input corresponding to the fundamental mode of a commercially available space division multiplexing unit based on Multi-Plane Light Conversion (MPLC) [18].

MPLC is a technique that allows to perform any unitary spatial transform. Theoretically, any unitary spatial transform can be implemented by a succession of transverse phase profiles separated by Optical Fourier Transforms (OFT). In particular, the conversion of N separate input Gaussian beams into N orthogonal propagation modes of a fiber, i.e. spatial multiplexing, can be considered as a unitary spatial transform and therefore can be achieved with MPLC. The unitarity of the transform ensures that there is no intrinsic loss in the mode conversion. Losses in MPLC only occur due to imperfect optical elements (e.g. coating or imperfect phase plate manufacturing). The inverse unitary

transform, given by using the MPLC in the reverse direction, implements the demultiplexing operation of the same modes. In order to reduce the footprint of the MPLC as well as decrease the complexity of aligning free-space optical elements, the MPLC is in practice implemented using a multi-pass cavity in which the successive phase profiles are all printed on a single reflective phase plate. The cavity is formed by a mirror and the reflective phase plate, implementing the successive phase profiles and optical transforms, to realize a given unitary spatial transform, with low optical losses and high modal selectivity. The optics can be adapted whatever the wavelength.

Although the MPLC has been here configured with Hermite-Gaussian modes (HG), it can address any spatial mode profile, in particular, Laguerre Gaussian (LG) beams, with high fidelity. We insert a $\pi/2$ converter based on cylindrical lenses before the MPLC unit, to convert LG beams into HG beams [19]. Then, the association of a mode converter and the spatial mode multiplexer multiplexes or demultiplexes into LG beams that have cylindrical symmetry. One has to note that here, the incoming fundamental beam remains unchanged by the MPLC and by this $\pi/2$ converter too. When the MPLC is used as a demultiplexer like here, the various LG beams are converted into fundamental modes and then injected independently in SMF 28 fibers, leading to fundamental modes that encounter little losses during propagation at the outputs. Each signal can be investigated independently. We can also mix these signals to a reference beam that has been frequency shifted with to acousto-optics modulators, thanks to coupler C_3 . The beat frequency is then sent to a spectrum analyzer (SA). Fig. 1 corresponds to a situation where we investigate the beat frequency between the fundamental beam and the shifted reference beam. In the case of higher orders LG beams, there is no need for the C_2 coupler. The output corresponding to the LG beam is directly connected to coupler C_3 .

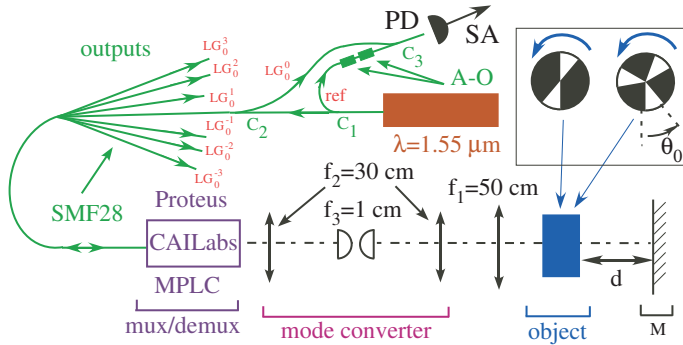


Fig. 1. Experimental set-up. CW laser source: $\lambda = 1.55\mu\text{m}$ connected to the input/output of the LG_0^0 mode of the MPLC. MPLC: spatial multiplexer or demultiplexer. $f_1=50\text{ cm}$: mode matching lens. $f_2=30\text{ cm}$: focusing lenses; distance between them 60 cm . $f_3=1\text{ cm}$: cylindrical lenses acting as a $\pi/2$ converter; distance between them 1.41 cm . M: fixed mirror. A-O: acousto-optic modulator. The outputs are fundamental beams that correspond to the LG beams that have been demultiplexed by the MPLC. PD: Photodiode; SA: towards Spectrum Analyzer; C_1, C_2, C_3 : fiber couplers. $d = 0.45\text{ m}$. The inset shows the rotating objects used: a two-blade and a three-blade propeller.

The incoming laser light at the output of the MPLC is focused on a plane mirror by a $f_1 = 50\text{ cm}$ lens that retro-reflects the light

to lens and the the MPLC unit (see Fig. 1). Thus the reflected beam is mode-matched to the fundamental beam of the MPLC. There are no particular difficulties in operating the MPLC. However, the mode matching condition has to be fulfilled. For that purpose, the fixed mirror M is mounted on a micro-stage linear translation, and the incidence angle can be adjusted thanks to two knob actuators. We check the mode matching condition by investigating the decomposition of the reflected beam on the LG basis (see Fig. 2a). After optimization, there is less than 1% light intensity in the non fundamental modes.

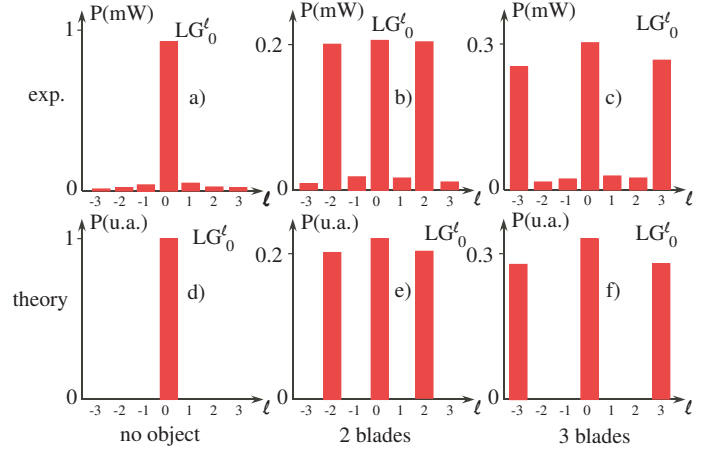


Fig. 2. Experimental a), b), c) and corresponding theoretical d), e), f) decomposition of the reflected light on a LG basis, with no object a), d), a two-blade propeller b), e), a three-blade propeller c), f). Note that the units are the same for the three theoretical curves.

3. RESULTS

We then insert a drawing printed on a transparency that only transmits light through precise angular sectors (see insert of Fig. 1). The drawing and the mirror together mimic the reflection of light on a two or three blades propeller. The positive sense of rotation of the object corresponds to a clockwise rotation of the phase of the electromagnetic field ($\ell > 0$) with respect to the direction of propagation of the incident light.

The reflected light doesn't correspond to the fundamental beam anymore. We decompose it in the LG basis considering the LG_0^ℓ , with $\ell = 0, \pm 1, \pm 2, \pm 3$ modes only. These are the available modes on our MPLC. Note that the waist of these modes is the same as the one of the fundamental mode, which is mode matched to the laser source. We check the topological charge using a double slit experiment [20]. Such an experimental decomposition is displayed in Fig. 2b and 2c. It is worth noting that for a two blade propeller with a π symmetry, apart from the fundamental mode, the dominant modes of the decomposition are the LG_0^{-2} , and LG_0^2 modes with nearly equal intensity, whereas for a three blade propeller with a $2\pi/3$ symmetry the dominant modes of the decomposition are the LG_0^{-3} , and LG_0^3 modes with nearly equal intensity. With higher LG modes available, the modes with a topological charge that is a multiple of the symmetry of the object would have also a significant contribution to the signal.

A. Theoretical considerations

Let us compare these experimental results with theoretical calculations. A LG_0^ℓ mode can be written as [21]

$$E^\ell(r, \theta, z) = A^\ell(r, z) e^{i\frac{kr^2}{2R(z)}} e^{i\ell\theta} e^{-i\varphi^\ell(z)} e^{i(kz - \omega t)} \quad (1)$$

with

$$A^\ell(r, z) = \sqrt{\frac{1}{\pi|\ell|!} \frac{\sqrt{P_0}}{w(z)} \left(\frac{r\sqrt{2}}{w(z)}\right)^{|\ell|} e^{-\frac{r^2}{w^2(z)}}} \quad (2)$$

(r, θ, z) are the cylindrical coordinates, ω is the wave pulsation and k is the wavevector. P_0 is the optical power, $w(z)$ is the waist of the beam at the z position, $R(z)$ is the radius of curvature of the beam. $\varphi^\ell(z) = (|\ell| + 1) \arctan(\frac{z}{z_R})$ is the Gouy phase and z_R is the Rayleigh zone [22]. We assume here that we are far from the Rayleigh zone and we thus neglect this Gouy phase.

In order to decompose the transmitted field, one has to calculate the overlap between the reflected field $E^0 f(\theta)$ ($f(\theta)$ being the reflection of the object, see below) and the LG_0^ℓ modes. Omitting diffraction, it writes

$$K^\ell = \int_0^\infty r dr \int_0^{2\pi} (E^\ell(r, \theta))^* E^0(r, \theta) f(\theta) d\theta \quad (3)$$

where $(\cdot)^*$ denotes the complex conjugate. Since without the propeller, the incident beam is mode matched to the fundamental beam, the two fields in Eq. 3 are evaluated at the same z position. They have the same waist and the same phase factor due to propagation and time dependance. The phase terms thus cancel in Eq. 3. $f(\theta) = 1$ for $-\theta_0 + \frac{2\pi m}{n} \leq \theta \leq \theta_0 + \frac{2\pi m}{n}$, and $f(\theta) = 0$ otherwise, n being the number of blades, $m = 0, \dots, n-1$, and $\theta_0 = 20^\circ$ in our experimental situation. This value is given as an example. Note that the rotational Doppler shift here is independent of the value chosen for θ . It only plays a role on the strength of the signal. Eq. 3 can be decomposed in a radial term that is calculated analytically, assuming that $P_0 = 1$

$$K_{rad}^\ell = \frac{1}{\pi\sqrt{2}} \sqrt{\frac{1}{|\ell|!}} \int_0^\infty u^{|\ell|} e^{-u^2} u du \quad (4)$$

where $u = \frac{2r^2}{w^2}$. For example, for $\ell = 0$, the radial term equals $1/(2\pi)$. There is also an angular part

$$K_{ang}^\ell = \int_0^{2\pi} f(\theta) e^{-i\ell\theta} d\theta = \sum_{m=0}^{n-1} \int_{-\theta_0 + \frac{2\pi m}{n}}^{\theta_0 + \frac{2\pi m}{n}} e^{-i\ell\theta} d\theta \quad (5)$$

It equals $2n\theta_0$ for $\ell = 0$. It equals $\frac{2n}{\ell} \sin(\ell\theta_0)$ when ℓ is a multiple of n and it is 0 otherwise. We can then plot the intensity of the modes of the decomposition ($|K^\ell|^2$). It is displayed on Fig. 2e and 2f. The agreement between the theoretical values and the experimental measurements is very good. It is worth noting that experiments aiming at rotational symmetry investigation in target identification usually use beams carrying Orbital Angular Momentum (OAM) as an incident beam [23], whereas in our case, the incoming beam is the fundamental beam that is much easier to generate and handle.

B. Object rotation

The drawing of the propellers is mounted on a homemade hollow shaft driven by a belt and a motor that has been carefully aligned with the optical axis in order to rotate the propeller at a constant velocity. Let us first consider a fixed given rotation of an angle θ_r . On a theoretical point of view, this rotation is

nothing but a translation of the origin of the angle. It induces an extra term $e^{i\ell\theta_r}$ in Eq. 5 that can be factorized, leading to a phase shift that equals $\ell\theta_r$, in the expression of the field of the LG_0^ℓ .

When the propeller is rotating at a constant angular velocity $\Omega_r = 2\pi\nu_r$, the phase shift varies in time and writes $\ell\Omega_r t$. It corresponds to a frequency shift of the electromagnetic field

$$\Delta\nu = -\ell\nu_r \quad (6)$$

which is in agreement with the rotational frequency shift [5, 7]. When the propeller rotates in the same sense as the phase of the LG beam ($\Omega_r > 0, \ell > 0$), the frequency of the LG electromagnetic field decreases (its frequency is red shifted). When the propeller rotates in the opposite sense as the phase of the LG beam ($\Omega_r < 0, \ell > 0$, or $\Omega_r > 0, \ell < 0$), the frequency of the LG electromagnetic field increases (its frequency is blue shifted).

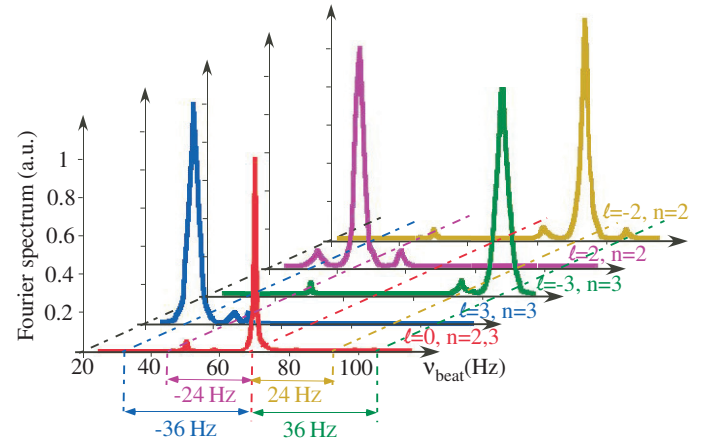


Fig. 3. Fourier analysis of the beat frequency between the reference beam (70 Hz shifted regarded to the laser frequency) and the LG_0^ℓ components of the decomposition, $\ell = -3, -2, 0, 2, 3$. The rotation frequency of the propeller is here equal to $\nu_r = 12$ Hz.

C. Rotational Doppler shift

Let us perform the experiment. Since the outputs of the MPLC are connected with fibers, we can easily measure the intensity of each mode. We check that the intensity variation for a single mode is nearly constant during the propeller rotation (less than a 5% modulation due to the rotation). We can also couple the LG_0^ℓ with a reference beam originating from the laser source. In order to perform a heterodyne measurement of the beat frequency, we shift the frequency of the reference beam from the laser source by 70 Hz thanks to two acousto-optic modulators. The Fourier transform, calculated numerically from the beat signal, is displayed on Fig. 3, for LG_0^ℓ ($\ell = 0, \pm 2, \pm 3$), for a n blade propeller ($n = 2, 3$) and for a rotation frequency of the shaft $\nu_r = 12$ Hz.

The fundamental mode LG_0^0 is not frequency shifted since the beat frequency corresponds to 70 Hz. The beat frequency between the LG_0^ℓ modes for $\ell = 2, 3$ and the reference signal equals $70 - 2 \times 12 = 46$ and $70 - 3 \times 12 = 34$ Hz, respectively. Their frequency is thus red shifted as expected. The beat frequency between the LG_0^ℓ modes for $\ell = -2, -3$ and the reference signal equals $70 + 2 \times 12 = 94$ and $70 + 3 \times 12 = 106$ Hz, respectively. The frequency is blue shifted in this case.

The frequency shift equals $\Delta\nu = -\ell\nu_r$, as expected, in very good agreement with Eq. 6. The peak corresponding to the beat

frequency between the reference and the LG_0^0 is rather sharp, limited by the sampling of the beat signal, whereas peaks corresponding to the beat frequency between the reference and the LG_0^ℓ modes for $\ell = 3, 2, -2, -3$ are broader. The main uncertainty on this beat frequency measurement relies on the precise determination of the rotation frequency of the propeller independently of the Doppler shift. It is estimated to 0.5 Hz. This then induces an uncertainty on the Doppler shift measurement, which is also of the same order.

Figure 4 shows the variation of the frequency shift versus the rotation frequency of the propeller. The only non zero contributions indeed correspond to modes having the same rotational property as the propeller. The frequency shift varies exactly linearly with the rotation frequency. This variation is in total agreement with the Doppler shift formula of Eq. 6. The part of the figure with a negative rotation frequency ν_r corresponds to a rotation of the propeller in the opposite direction.

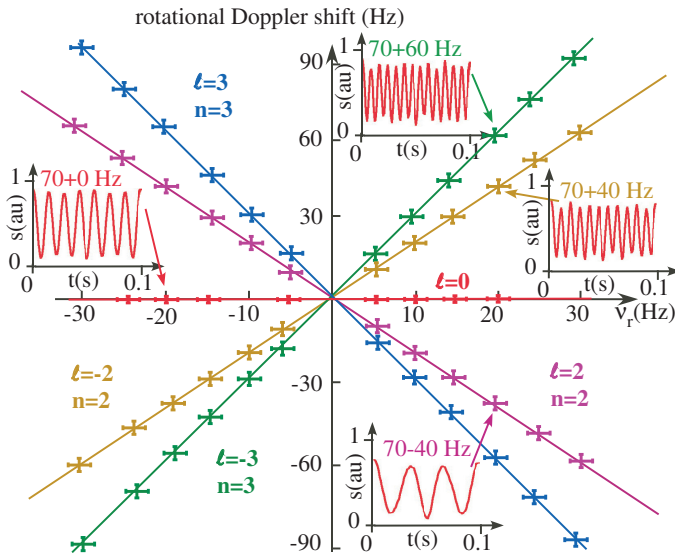


Fig. 4. Rotational Doppler shift of the LG_0^ℓ components, $\ell = -3, -2, 0, 2, 3$, versus the rotation frequency of the propeller. The size of the cross corresponds to the error bars. Inserts: beat frequency signal (s) in arbitrary units for a $\nu_r = 20$ Hz rotation frequency. The frequency beat equals 70 Hz plus the rotational Doppler shift.

In our experiment, the rotating object and the fixed mirror together, mimic a reflection from a propeller. However, as the light passes twice through the object, one may wonder whether it could induce a cascade Doppler effect [24]. This is not the case for the following reason. The distance between the object and the mirror is $d = 0.45$ m. The time for the light to travel from the object to the mirror and back to the object is $\tau = 2d/c$, c being the velocity of light. Meanwhile, the rotation of the object is $\alpha = \Omega_r \tau$, which is very small. Then, the reflected light exactly matches the object. This has no influence on the experiment. In the case of a longer distance d , since the transmitted and then reflected light has the same rotational symmetry as the rotating object, the reflected light after the object would keep the same the rotational symmetry as before. There would be no extra, nor cascade Doppler effect. In the absence of such a mirror, the system corresponds to a bistatic radar system with a rotational Doppler effect as explained in [17].

4. DISCUSSION

Conceptually, the experiment performed here is very different from most of the experiments proposed or realized on rotational Doppler effect in reflection, up to now. Most of the time, an OAM beam is shined on a surface that changes the topological charge of the beam [8–11, 14]. This also includes dedicated metasurfaces [12] that changes the angular momentum (spin, OAM or both) of the incoming beam. The detection is then performed on the reflected light. Here, the incoming is the usual fundamental beam. It doesn't carry any OAM. The reflecting propeller is also an ordinary surface. It doesn't operate any topological charge transformation like the ones performed with spiral phase plates, phase conjugated mirrors, or helicoidal reflectors [11, 13, 24]. As soon as the reflected beam doesn't correspond to the fundamental beam and could be decomposed in a LG basis, the non-zero LG beams do experience a rotational Doppler shift that could be detected. Such an experimental set up is easy to handle and versatile.

This kind of rotational Doppler shift measurement is not limited to optics. It could be adapted to any electromagnetic wavelength depending on the desired application and could be generalized to any wave including acoustic waves [25]. Perhaps, the most promising part relies in the radar spectrum of the electromagnetic waves where OAM waves have been evidenced [26]. All the existing applications of the linear Doppler radar investigation can be readily applied to rotating systems using the rotational Doppler shift the way we did. Distorsion of the wavefront due to atmospheric perturbation for example could be corrected [27]. Besides, by using a green laser for example, it could be possible to identify the numbers of blades and the rotation speed of a submarine propeller. Indeed, the monitoring of rotating systems, including marines and aircraft propellers and wind turbines is still a very complex issue [28]. The rotating Doppler shift measurement, as it has been performed here can offer new decisive ways to tackle this problem.

As pointed out by Padgett [29], the rotational Doppler effect is associated with the power of the applied torque. It must result in a frequency shift and consequently, in a change of the total energy of the field. Due to energy conservation [30], this energy change of the field must be compensated for a change of energy of the object. Conversely, the rotation of an object must lead to a change of the electromagnetic field [31]. However, here, since the LG beams with opposite charge are shifted with opposite sign, there is no change of the total OAM of the beam. There is thus no torque. The rotation measurement is then non invasive regarded to the rotation itself.

5. CONCLUSION

To conclude, we have investigated the structure of the light reflected by an object mimicking a propeller. We have decomposed the light in a LG basis using a commercially available MPLC. Only the modes having the same rotational symmetry as the object have a significant contribution. We have isolated a rotational Doppler shift on each of these LG modes. The shift equals the topological charge times the rotational frequency of the object. The modes having the phase rotating in the same sense as the object are red shifted, whereas the other modes are blue shifted.

We have mainly mentioned promising applications in the radar domain for remote identification of rotation of macroscopic objects such as propellers and turbine. Nevertheless this work could also find applications in the micro and nano world. Actually, there is an increasing need to fully characterize the

dynamics of micro/nanomotors that are used as microrobotics in drug delivery for biomedical applications [32, 33]. A MPLC coupled with a microscope could monitor and fully characterize the dynamics of such motors.

Funding. No funding sources.

Acknowledgments. We wish to acknowledge technical support from X. Morvan and J.-R. Thébault.

Disclosures. The authors declare no conflicts of interest.

Data availability. Data underlying the results presented in this paper are not publicly available at this time but may be obtained from the authors upon reasonable request.

REFERENCES

1. R. J. Sullivan and R. D. Sullivan, *Radar foundations for imaging and advanced concepts*, vol. 2 (SciTech Publishing, Raleigh, NC, USA, 2004).
2. M. Cheney and B. Borden, *Fundamentals of radar imaging* (SIAM, Philadelphia, USA, 2009).
3. D. Tahmouh, "Review of micro-doppler signatures," *IET Radar Sonar Navig.* **9**, 1140–1146 (2015).
4. V. C. Chen, *The micro-Doppler effect in radar* (Artech House, Boston/London, 2019).
5. M. Padgett, "Like a speeding watch," *Nature* **443**, 924–925 (2006).
6. L. Marrucci, "Spinning the doppler effect," *Science* **341**, 464–465 (2013).
7. L. Fang, M. J. Padgett, and J. Wang, "Sharing a common origin between the rotational and linear doppler effects," *Laser Photon. Rev.* **11**, 1700183 (2017).
8. M. P. Lavery, F. C. Speirits, S. M. Barnett, and M. J. Padgett, "Detection of a spinning object using light's orbital angular momentum," *Science* **341**, 537–540 (2013).
9. A. Ryabtsev, S. Pouya, A. Safaripour, M. Koochesfahani, and M. Dantus, "Fluid flow vorticity measurement using laser beams with orbital angular momentum," *Opt. Express* **24**, 11762–11767 (2016).
10. S. Qiu, Y. Ren, Q. Sha, Y. Ding, C. Wang, Z. Li, and T. Liu, "Observation of the rotational doppler shift of the ring airy gaussian vortex beam," *Opt. Commun.* **490**, 126900 (2021).
11. A. Y. Okulov, "Rotational doppler shift of a phase-conjugated photon," *J. Opt. Soc. Am. B* **29**, 714–718 (2012).
12. P. Georgi, C. Schlickriede, G. Li, S. Zhang, and T. Zentgraf, "Rotational doppler shift induced by spin-orbit coupling of light at spinning metasurfaces," *Optica* **4**, 1000–1005 (2017).
13. B. Liu, H. Chu, H. Giddens, R. Li, and Y. Hao, "Experimental observation of linear and rotational doppler shifts from several designer surfaces," *Sci. Rep.* **9**, 1–9 (2019).
14. O. Emile, J. Emile, and C. Brousseau, "Rotational doppler shift upon reflection from a right angle prism," *Appl. Phys. Lett.* **116**, 221102 (2020).
15. W. Zhang, J. Gao, D. Zhang, Y. He, T. Xu, R. Fickler, and L. Chen, "Free-space remote sensing of rotation at the photon-counting level," *Phys. Rev. Appl.* **10**, 044014 (2018).
16. O. Emile, J. Emile, C. Brousseau, T. le Guennic, and P. Jian, "Rotational doppler shift from a rotating rod," *Opt. Lett.* **46**, 3765–3768 (2021).
17. O. Emile, J. Emile, C. Brousseau, T. le Guennic, and P. Jian, "Rotational doppler shift of the light transmitted behind a rotating object with rotational symmetries: rotational doppler shift of the transmitted light," *Eur. Phys. J. D* **76**, 8 (2022).
18. G. Labroille, B. Denolle, P. Jian, P. Genevieux, N. Treps, and J.-F. Morizur, "Efficient and mode selective spatial mode multiplexer based on multi-plane light conversion," *Opt. Express* **22**, 15599–15607 (2014).
19. J. Courtial and M. Padgett, "Performance of a cylindrical lens mode converter for producing laguerre–gaussian laser modes," *Opt. Commun.* **159**, 13–18 (1999).
20. O. Emile and J. Emile, "Young's double-slit interference pattern from a twisted beam," *Appl. Phys. B* **117**, 487–491 (2014).
21. G. Molina-Terriza, J. P. Torres, and L. Torner, "Twisted photons," *Nat. Phys.* **3**, 305–310 (2007).
22. A. E. Siegman, *Lasers* (University Science Books, 1986).
23. N. Uribe-Patarroyo, A. Fraine, D. S. Simon, O. Minaeva, and A. V. Sergienko, "Object identification using correlated orbital angular momentum states," *Phys. Rev. Lett.* **110**, 043601 (2013).
24. Z. Guo, J. Meng, M. An, P. Cheng, J. Jia, Z. Chang, X. Wang, and P. Zhang, "Remote angular velocity measurement by the cascaded rotational doppler effect," *Appl. Opt.* **60**, 9892–9895 (2021).
25. G. M. Gibson, E. Toninelli, S. A. Horsley, G. C. Spalding, E. Hendry, D. B. Phillips, and M. J. Padgett, "Reversal of orbital angular momentum arising from an extreme doppler shift," *Proc. Natl. Acad. Sci.* **115**, 3800–3803 (2018).
26. B. Thidé, H. Then, J. Sjöholm, K. Palmer, J. Bergman, T. Carozzi, Y. N. Istomin, N. Ibragimov, and R. Khamitova, "Utilization of photon orbital angular momentum in the low-frequency radio domain," *Phys. Rev. Lett.* **99**, 087701 (2007).
27. S. Li, S. Chen, C. Gao, A. E. Willner, and J. Wang, "Atmospheric turbulence compensation in orbital angular momentum communications: Advances and perspectives," *Opt. Commun.* **408**, 68–81 (2018).
28. G. Genta, *Dynamics of rotating systems* (Springer Science & Business Media, New York, 2007).
29. M. Padgett, "Light's twist," *Proc. Math. Phys. Eng. Sci.* **470**, 20140633 (2014).
30. O. Emile and J. Emile, "Energy, linear momentum, and angular momentum of light: What do we measure?" *Ann. Phys.* **530**, 1800111 (2018).
31. O. Emile, C. Brousseau, J. Emile, R. Niemiec, K. Madhjoubi, and B. Thidé, "Electromagnetically induced torque on a large ring in the microwave range," *Phys. Rev. Lett.* **112**, 053902 (2014).
32. T. Li, M. Wan, and C. Mao, "Research progress of micro/nanomotors for cancer treatment," *ChemPlusChem* **85**, 2586–2598 (2020).
33. Q. Yang, L. Xu, W. Zhong, Q. Yan, Y. Gao, W. Hong, Y. She, and G. Yang, "Recent advances in motion control of micro/nanomotors," *Adv. Intell. Syst.* **2**, 2000049 (2020).